Journal of Photochemistry and Photobiology A: Chemistry 222 (2011) 123–131

Contents lists available at ScienceDirect

Journal of Photochemistry and Photobiology A: Chemistry

journal homepage: www.elsevier.com/locate/jphotochem

Adsorption and photocatalytic degradation of human serum albumin on TiO_2 and Ag–TiO_2 films

Mukhtar H. Ahmed[a,b,*], Tia E. Keyes[a], John. A. Byrne[b], Charles W. Blackledge[a], Jeremy. W. Hamilton[b]

[a] School of Chemical Science, National Centre for Sensor Research (NCRS), Dublin City University, Dublin 9, Ireland
[b] Nanotechnology and Integrated Bio-Engineering Centre (NIBEC), University of Ulster, Jordanstown, BT37 0QB Belfast, UK

ARTICLE INFO

Article history:
Received 3 February 2011
Received in revised form 13 May 2011
Accepted 21 May 2011
Available online 6 June 2011

Keywords:
TiO_2
Ag–TiO_2
Photocatalytic activity
Protein
Adsorption
Degradation

ABSTRACT

Titanium dioxide is a useful material in the biomedical field as it has excellent biocompatibility based on its non-toxicity and non-inflammatory properties. Furthermore, TiO_2 can be excited by UV light to create charge carriers giving rise to photocatalytic redox reactions at the surface and photo-induced super-hydrophilicity. These properties might be exploited for surface decontamination of medical devices and implants. With this in mind, titanium dioxide TiO_2 films were prepared on stainless steel substrates using magnetron sputtering. Silver loaded (Ag–TiO_2) films were prepared by the photocatalytic reduction of Ag^+ from solution. The adsorption of human serum albumin (HSA) was studied. Surface analysis methods used included X-ray diffraction (XRD), X-ray photoelectron spectroscopy (XPS), Raman spectroscopy and atomic force microscopy (AFM). The TiO_2 films were predominantly anatase crystal phase and the photoreduced Ag was present at greater than 90% of the silver content as Ag^0 on the surface. Ag loading of the TiO_2 markedly enhanced the Raman signal (ca. 15-fold), but caused significant changes to the spectrum indicating non-specific binding of protein side chain residues to the Ag. The amide I and III modes remained well-resolved and were used to estimate the conformational change induced by the Ag. Raman analysis showed an increase in the intensity of the band at ~1665 cm^{-1} assigned to the disordered conformation, suggesting that the adsorption to the Ag sites induces conformational changes in the protein. UVB irradiation of the protein contaminated surfaces caused further changes in the protein conformation, consistent with denaturation and enhanced binding and oxidation, thought to be induced through a photocatalytic mechanism.

1. Introduction

Interfacial adsorption of proteins is a key issue in medicine with respect to the contamination of surgical instruments and the biocompatibility of medical implants. The nature of adsorption and the impact this event has on the structure of the protein varies widely depending on the properties of both the protein and the interface. Reliable strategies for desorption or denaturation of proteins adsorbed at a surface are critically important for the decontamination of surfaces of surgical instruments which may have been contaminated with infectious materials, for example, prion protein.

Among metallic materials used in biomedical applications, titanium and its alloys are probably the most important due to their chemical stability, low mass, high strength, corrosion resistance, and their excellent biocompatibility [1]. *In vitro* and *in vivo* experiments have demonstrated that titanium dioxide coatings exhibit good blood compatibility [2–4] and do not appear to induce platelet aggregation, damage red blood cells or adsorb fibrin strongly [5]. Consequently, titanium and its alloys are used in dental, orthopaedic and cardiovascular implants [5,6]. The biocompatibility of titanium and its alloys is associated with the properties of the titanium surface oxides [7–9].

Like titanium, stainless steel is widely used in medical devices and instruments, because of its low cost and its strength. Surgical steel is regarded as easy to sterilize; however, protein adsorbates, most critically prion protein, may not be totally removed by conventional sterilization procedures [10].

Titanium dioxide (TiO_2) is an excellent photocatalyst [11]. The anatase form is a wide band gap (3.2 eV) semiconductor that can be excited under UV irradiation to produce electron hole pairs. These photogenerated charge carriers can either recombine or react with a species at the surface of the TiO_2. If in contact with an aqueous environment, the hole will take an electron from water or hydroxide ion to form hydroxyl radicals. If oxygen is present, it can act as an electron accepter forming superoxide radical anion. In this way, reactive oxygen species are formed which can attack and degrade

* Corresponding author at: Nanotechnology and Integrated Bio-Engineering Centre (NIBEC), University of Ulster, Jordanstown, BT37 0QB Belfast, UK.
Tel.: +44 0 2890368942.
E-mail address: ahmed-m@email.ulster.ac.uk (M.H. Ahmed).

1010-6030/$ – see front matter © 2011 Elsevier B.V. All rights reserved.
doi:10.1016/j.jphotochem.2011.05.011

organic material present at or near the interface [12,13]. TiO_2 photocatalysis has been reported to be effective for the degradation of a wide range of organic chemicals in water and air, and for the inactivation of microorganisms including viruses, bacteria and protozoa [14,15]. TiO_2 films can be deposited by a range of physicochemical methods including sputtering, CVD, sol–gel synthesis and immobilisation of nanoparticles [16–18].

Silver loaded TiO_2 has previously been reported to act as a good substrate for surface enhanced Raman (SERS) [19,20]. Furthermore, loading the surface of TiO_2 with metal clusters can also enhance the photocatalytic activity by providing sites for charge carrier separation, improving electron or hole transfer to solution i.e. electro-catalysis, and/or by providing more surface area for adsorption [20–22]. Ag may be deposited onto TiO_2 surfaces via various physicochemical routes, including photocatalyic reduction where Ag^+ is reduced at the surface of the TiO_2 by photogenerated electrons [9,17,19].

Silver in itself has interesting biological properties. For example, it is possible to improve the biocompatibility of artificial blood vessels by coating with silver [23]. Compared with other metals, silver exhibits higher toxicity to microorganisms while it exhibits lower toxicity to mammalian cells [24].

In this contribution, we explore the coating of stainless steel with TiO_2 thin films and subsequent loading of these films with Ag particles. The adsorption of protein on these substrates is investigated along with the photocatalytic decomposition of protein under ultraviolet irradiation. TiO_2 films were prepared on 316 stainless steel coupons using magnetron sputtering. Ag–TiO_2 was prepared by photocatalytic reduction of Ag^+ from solution. The protein model explored was human serum albumin since its adsorption onto surgical instruments and medical devices is likely to dominate *in vivo* due to its abundance in human serum. The films were characterised using advanced surface analytical techniques, including Raman spectroscopy, X-ray photoelectron spectroscopy (XPS), X-ray diffraction (XRD) and atomic force microscopy (AFM).

2. Experimental

2.1. Preparation of TiO_2 thin films

Polished coupons of 316 stainless steel ($2 \times 2\ cm^2$) were cleaned using acetone in an ultrasonic water bath for 30 min, then washed using distilled water and dried with nitrogen gas. TiO_2 thin films were then deposited on the clean coupons by radio-frequency (rf) magnetron sputtering using an unbalanced magnetron system (TEER UDP 450). Sputtering was carried out in an argon and oxygen plasma, with a Ti target (Teer, 99.6% pure) and pressure $<5 \times 10^{-6}$ Pa. The deposition process was performed in power regulation mode at 400 W, resulting in 0.96 A applied to the target. The partial pressures of oxygen and argon were controlled by the oxygen and argon flow rates. A ratio of 15 sccm argon to 5 sccm oxygen led to a concentration of oxygen of around 25%. The time of deposition was around 8 h. The thickness of the deposited TiO_2 layers was estimated using stylus profilometry measurements. To improve the crystallinity of the TiO_2 films, some samples were annealed at elevated temperatures in air (samples were heated at a rate of 5 °C /min to a temperature of 430 °C, held for 3 h, and cooled at 5 °C/min).

2.2. Photo-reduction of Ag onto TiO_2 films

Samples were placed in a Petri-dish, with the TiO_2 film facing upwards, and immersed in a 75:25, v/v CH_3OH:H_2O solution containing 0.001 M of $AgNO_3$. The films were then irradiated over different intervals ranging between 10 and 60 min using a UV-A fluorescent lamp (Philips, PLS 9 W) set 6 cm above the Petri dish. The samples were then washed with distilled water, dried under a stream of nitrogen and stored in the dark.

2.3. Silver ion release from the Ag/TiO_2 thin film

ASV was used for the quantitative determination of the silver ion concentration releasing from the Ag/TiO_2 films, and measurements of various solutions with a defined silver ion concentration led to a calibration curve [25,26]. Prepared samples of Ag/TiO_2 thin film 2 cm × 2 cm × 0.1 cm in size was immersed into a sealable tube containing 15 mL of distilled water (DW). Then, the tube was oscillated at 37 °C in a water bath. One millilitre from above storage solution was taken out at interval of 1, 3, 5, 7, 10 and 15 days. The ASV measurements for silver ion release were carried out using an Autolab PGSTAT 20 (ECO CHEMIE), using a conventional three-electrode electrochemical cell containing a glass carbon electrode and a Pt wire as working and counter electrodes, respectively. Ag/AgCl electrodes with saturated KCl solution were employed as reference electrodes. The detail experiments are described by Liu and Kumar et al. other co-workers [26,27].

2.4. Protein adsorption

Solutions of human serum albumin (HSA, 0.5%, w/v) were prepared in distilled water (phosphate buffer saline (PBS) was not used to avoid interference from phosphate ion which binds strongly to the surface of TiO_2). Both TiO_2 and Ag–TiO_2 samples were treated in the same way and immersed in the HSA solution for 30 min in Petri dishes, after which they were removed, washed and dried.

2.5. UV-photocatalysis

Following exposure to HSA, samples were irradiated using either UV-A or UV-B, to determine the effect of photocatalysis on the protein structure. The UV-A source was a fluorescent lamp (Philips, PLS 9 W/10) set 6 cm above the Petri dish, with peak emission at ~365 nm. The UVB source was a fluorescent lamp (Philips, PLS 9 W/12/2p) set 6 cm above the Petri dish with peak emission at 315 nm. Dark and light control experiments were also undertaken.

2.6. Film characterisation

A Bruker D8 X-ray diffractometer was used for powder XRD analysis. Diffraction patterns were collected in reflection-mode geometry from 20° to 80° 2θ at a rate of 0.05° 2θ/min. XPS analysis was undertaken using an AXIS Ultra XPS system using a monochromatic Al Kα X-ray source ($h\nu$ 1486 eV) generated from an aluminium anode operating at an emission voltage of (15 kV) with current of 5 mA at the source.

Raman spectra were recorded on a Horiba Jobin Yvon HR800UV microscope using ~2 mW from a 532 nm laser diode for excitation and the following parameters, confocal aperature 200 μm, spectral resolution ~5 cm^{-1}. A 100× objective was employed and typical acquisition times were 5 s with 7 time repeat. This process was repeated at four or five different spots across the samples of TiO_2 and Ag–TiO_2 to assess uniformity of response. Prior to acquisition the spectrometer was calibrated using the zero order diffraction peak and first order peak from a silicon phonon mode from a silicon wafer sample.

Atomic force microscopy (AFM) was performed on a multimode atomic force microscope (Digital Instruments, Veeco). The AFM exhibited a maximum scan area of 10 μm × 10 μm and a vertical range of 3 μm and was calibrated using calibration gratings purchased from Micro Masch, the force applied was 500 mV.

3. Results and discussion

3.1. TiO_2 and Ag–TiO_2 film characterisation

Samples of TiO_2 and Ag–TiO_2 films on stainless steel were annealed at 430 °C for 3 h to generate polycrystalline films. The film thicknesses have been achieved using profilometry, and the values were ~(100 ± 5) nm, the growth rate of film deposition was around (12 nm/h).

3.1.1. X-ray diffraction

X-ray diffraction (XRD) analysis was undertaken on both the TiO_2 and Ag–TiO_2 films. For TiO_2, the major peaks were observed at 2θ values of 25.3°, 48.2°, 53.9°, 55.0° and 62.6° which are assigned to (1 0 1), (2 0 0), (2 2 0), (1 0 5), (2 1 1) and (2 0 4) reflections of anatase (Fig. 1) [28]. For Ag–TiO_2 films, four additional diffraction peaks were observed at ca. 2θ = 38.3°, 44.1°, 64.7° and 77.5° assigned to (1 1 1), (2 0 0), (2 2 0) and (3 1 1) reflections of Ag particles, respectively (Fig. 1). This provides good evidence that silver metal is deposited on the surface of the TiO_2 by photocatalytic reduction (Eq. (1)):

$$2Ag^+ + CH_3OH \xrightarrow{TiO_2 \& h\nu (UV)} 2Ag^0 + CH_2O + 2H^+ \quad (1)$$

Also, it was observed that peaks at 2θ = 25.3°, 48° and 54° appeared when the Ag atomic ratio on the surface was above ~9.6% [28]. In addition, the intensity of peak at 38.3° increased with increasing irradiation time during the photo-reduction of Ag^+.

3.1.2. Raman spectra

The Raman spectra of TiO_2 and Ag–TiO_2 films are shown in Fig. 2. The observed modes are consistent with anatase TiO_2, where Raman active Ti–O stretching modes were observed at 636 cm^{-1} (E_g) and 515 cm^{-1} (A_{1g}), while O–Ti–O bending type vibrations were observed at 400 cm^{-1} (B_{1g}) and 152 cm^{-1} (E_g) [29]. Notably, there was no evidence for the presence of rutile TiO_2 which is characterised by modes at 606, 434 and 230 cm^{-1}. The Raman data correlates well with the XRD data, indicating that the TiO_2 is in the anatase phase. The results are similar to those reported by Sousa et al. [5]. Ag loading of the TiO_2 surface resulted in an enhancement of Raman signal intensity for TiO_2 modes along with the appearance of new bands at ~814 and 935 cm^{-1} which correspond to the silver metal (Ag^0) surface modes and Ag–OH bending mode, respectively [30].

3.1.3. X-ray photoelectron spectroscopy

Fig. 3 shows the high resolution XPS spectrum survey scan of TiO_2 and Ag–TiO_2 (4.7 at.%) films. Two peaks in the Ti 2p binding

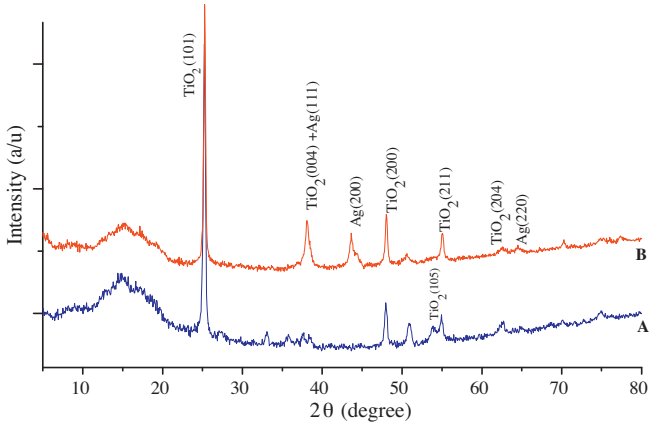

Fig. 1. XRD of TiO_2 (A) and 4.7 at.% Ag–TiO_2 (B) thin films.

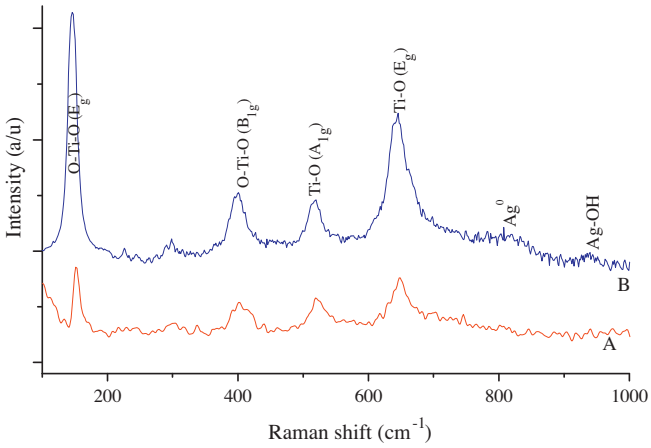

Fig. 2. Raman spectra for TiO_2 (A) and 4.7 at.% Ag–TiO_2 (B) thin films.

energy region were observed. The peak located at 464.7 eV can be assigned to Ti ($2p^{1/2}$) and the peak located at 458.4 eV corresponds to Ti($2p^{3/2}$). The splitting between both Ti ($2p^{1/2}$) and Ti ($2p^{3/2}$) core levels is around 5.7 eV, indicative of Ti^{4+} in the anatase phase of the TiO_2 film [12,31]. Peak de-convolution yielded three Gaussian peaks of Ti $2p^{3/2}$ at 457.2, 457.9 and 458.6 eV, and these were assigned to TiO, Ti_2O_3 and TiO_2, respectively [32]. The band at 458.6 eV correlating to TiO_2 contributes 89% of the Ti signal, as compared with the other bands for TiO (4%) and Ti^{3+} (7%) which can be resulted from the incorporation of silver and silver oxides on the TiO_2 layer [25] (Fig. 4A). Deconvolution of the O (1s) peak yielded three Gaussian components (Fig. 4B).

The lower binding energy peak is located at 530.8 eV and corresponds to the lattice oxygen of the TiO_2. The second component at 531.8 eV may be due to physisorbed water or –OH groups on the surface in –Ti(OH)–O–Ti–(OH)–. The highest binding energy peak at 527.0 eV, corresponds to C=O of (COH_2) which formed by photocatalytic deposition of silver and adsorbed oxygen on the surface. The O/Ti molar ratio of the film was calculated to be ~1.8 from the ratio of the peak areas [31,32].

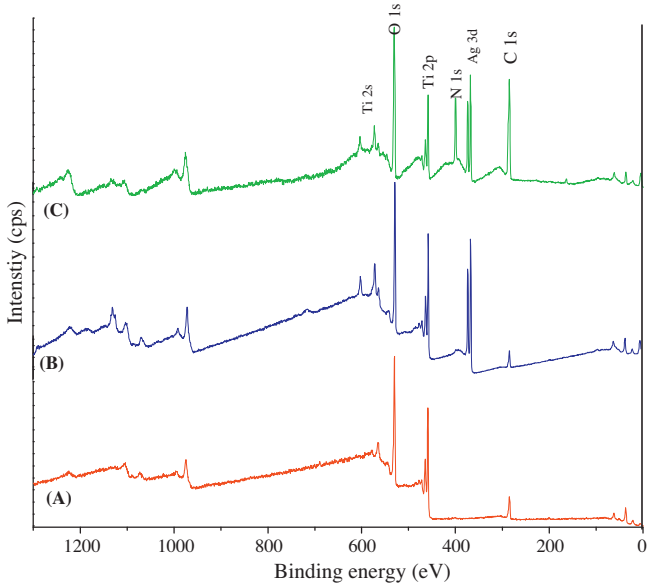

Fig. 3. XPS survey scan of TiO_2 (A), 4.7 at.% Ag–TiO_2 (B), HSA on Ag–TiO_2 (C).

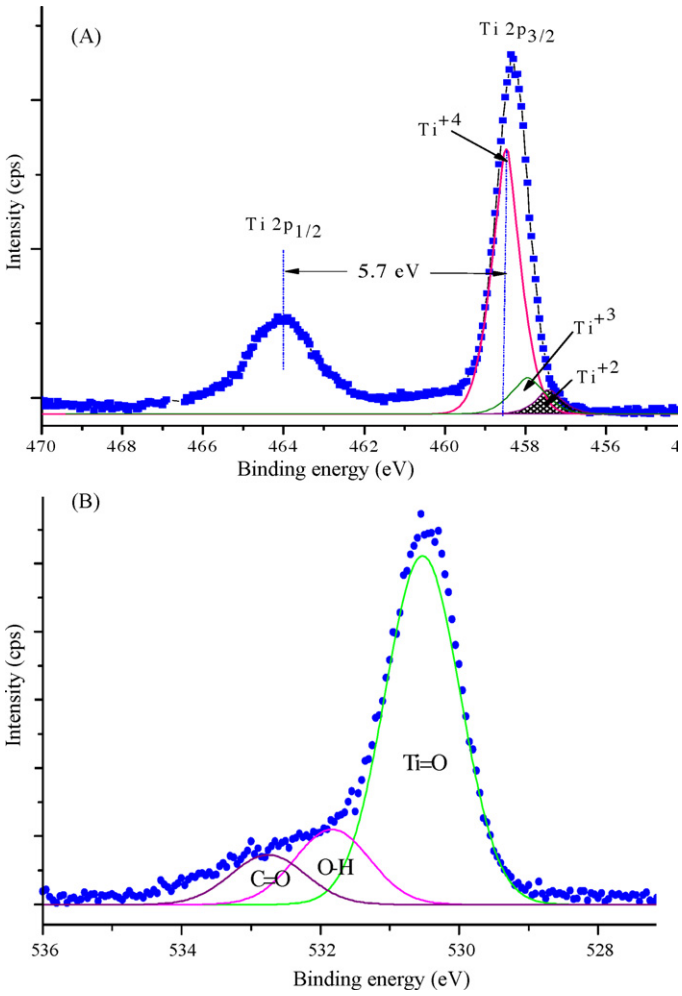

Fig. 4. XPS de-convolution of Ti 2p (A), O 1s (B) bands of TiO_2 thin film.

From the XPS survey scan of the Ag–TiO_2 films (Fig. 3B) additional bands attributed to TiO_2 film (Ti 2p and O 1s) appeared following silver loading and a new band was obtained at ~368 eV which is assigned to Ag 3d. Fig. 5 shows the Ag 3d spectrum with the Ag ($3d^{5/2}$) and Ag ($3d^{3/2}$) bands at 368.5 eV and 374.5 eV, respectively. The difference in energy between the 3d doublet is around 6.0 eV, indicating formation of metallic silver nanoparticles [31]. Peak deconvolution of the Ag (3d) band yielded three Gaussian peaks at 367.3, 367.8 and 368.5 eV corresponding to AgO, Ag_2O and Ag^0, respectively, however, Ag^0 is dominant (92%) with small contributions from Ag^+ (6%) and Ag^{+2} (2%). This correlates well with other reports [31,32].

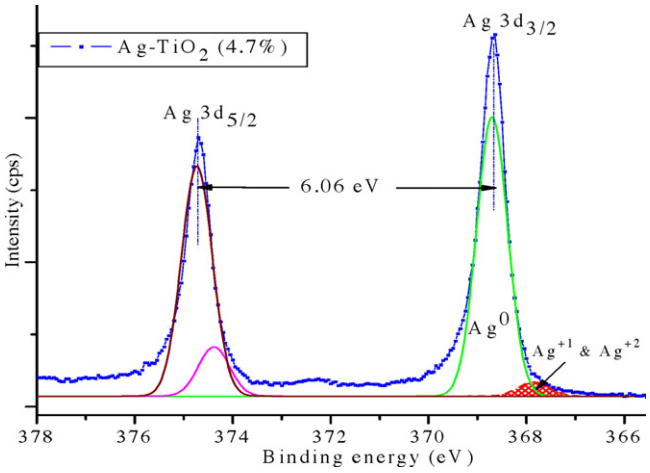

Fig. 5. XPS de-convolution of Ag 3d band of 4.7 at.% Ag–TiO_2 thin film.

3.1.4. Atomic force microscopy

Fig. 6(A and B) shows the AFM images of both of TiO_2 surface and silver nanoparticles grown on the TiO_2 films, respectively. The roughness was measured by the root mean square (rms) value (R_q) and it was ~23.2 ± 2.7 nm. The surface roughness was observed to slightly decrease on addition of Ag deposition whereby an rms of ~21.2 ± 1.6 for 4.7% Ag loading on the film, was recorded. The results are in good agreement with those reported by Malagutti et al. who found the surface roughness of TiO_2 film decreased with low deposition of silver [33].

3.1.5. Silver ion release from Ag/TiO_2 thin film

We have evaluated the silver ion release characteristics from Ag/TiO_2 films (which is a unique property of the antibacterial activity of silver doped TiO_2). The calibration curve is obtained by plotting the silver ion concentration of the corresponding standard solution of silver (Ag^+) as a function of current. Fig. 7 shows the concentrations of the released silver ions as a function of immersion time in DW. It can be seen that the concentrations of silver ion increases sharply and fastest release rate in the first seven days. The sharp initial release process of silver ions can be assigned to easy diffusion of water on the surfaces not effectively covered by the thin TiO_2 cap layer [32]. From day 7 to day 15 as we investigated, the release of Ag^+ becomes much steady. These results are similar to those of Wu et al. [34]. At these conditions, the saturated amount of released silver ions was measured nearly 1.8 μmol/L after 15 days, as can be seen in Fig. 7. This shows that the synthesised Ag/TiO_2 nanocomposite thin film can protect the immobilised silver nanoparticles for a long time [25].

Table 1
Raman shift and percentage of amide I band.

Bands	Samples							
	Random coil		α-Helices		β-Sheet		β-Turn	
	cm^{-1}	%	cm^{-1}	%	cm^{-1}	%	cm^{-1}	%
HSA free[a]	1637	11	1655	55	1669	22	1687	12
HSA on TiO_2 (dark control)	1635	12.8	1652	48.4	1671	30.2	1688	8.6
HSA on stainless steel + (UV-B)	1633	14.5	1653	47.3	1672	30.8	1689	7.4
HSA on TiO_2 + (UV-B)	1634	18.1	1654	45.6	1674	29.1	1688	7.2
HSA on 4.7 at.% Ag–TiO_2 + (UV-B)	1634	21.7	1654	42.7	1674	27.2	1688	8.4

HSA: Human serum albumin.
[a] Percentages obtained in Refs. [37,38].

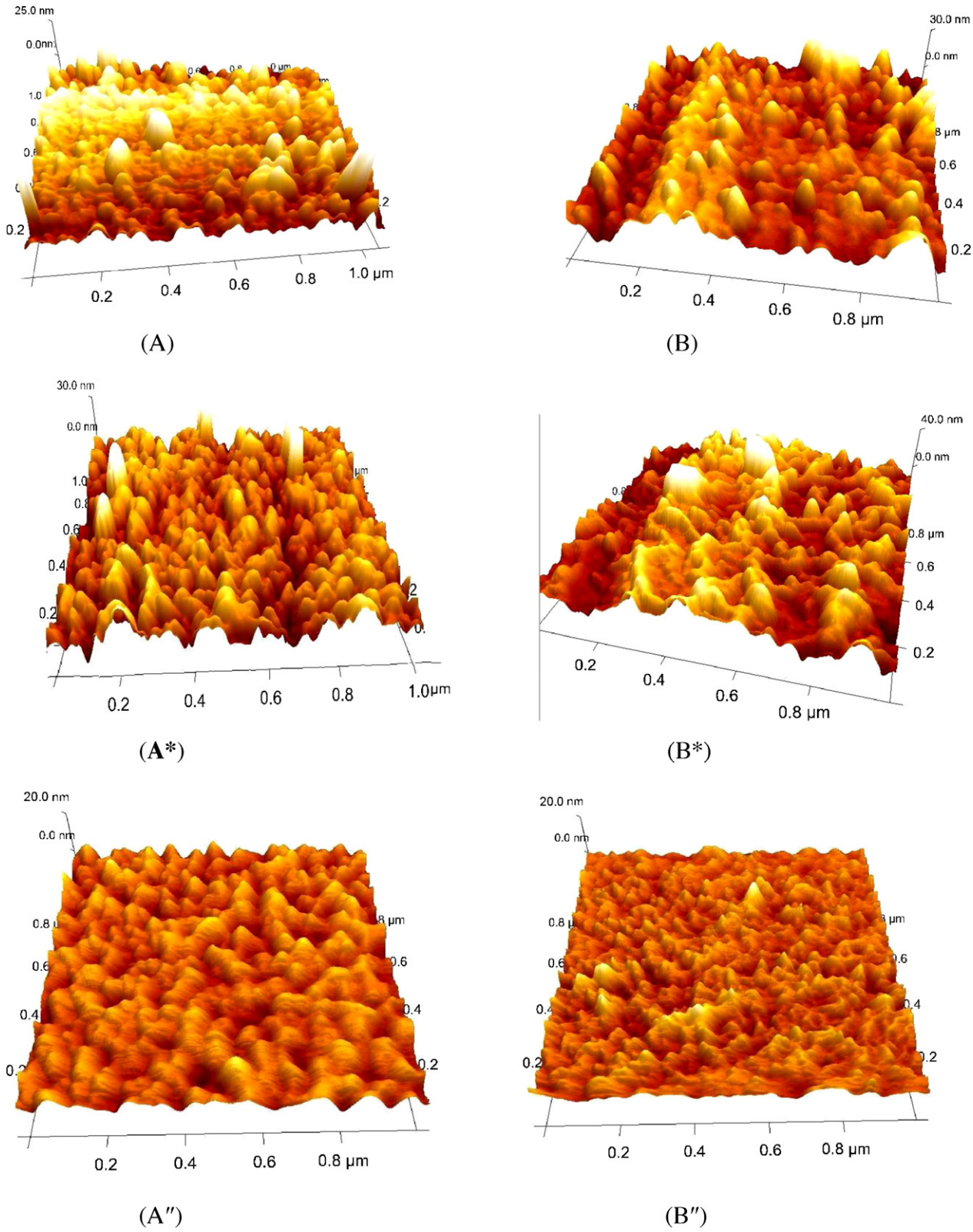

Fig. 6. AFM image of TiO_2 (A) and 4.7 at.% Ag–TiO_2 (B) before, after adsorption of HSA (A*), (B*), and following irradiation by UV-B (A″), (B″).

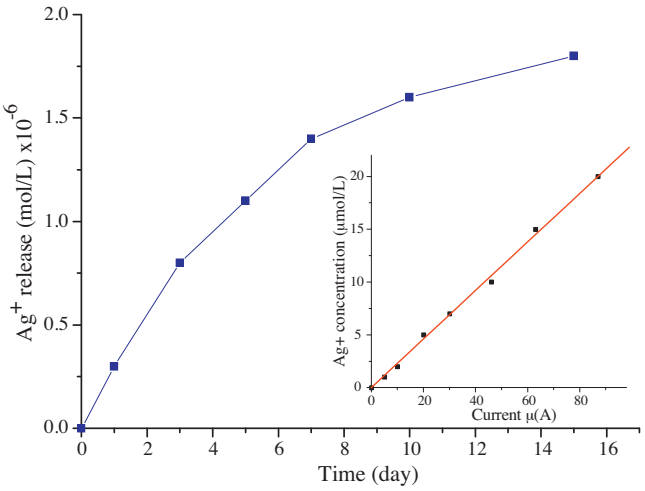

Fig. 7. Silver ion release curve of the 4.7 at.% Ag/TiO_2 thin film. The inset plot shows the obtained calibration curve of silver ions.

3.2. Protein adsorption

3.2.1. Raman of HSA–TiO_2

Fig. 8B shows the Raman shift of HSA adsorbed on the TiO_2 surface. The amide I band is centred at ~1660 cm^{-1}, and there is a well resolved peak between 1230 and 1340 cm^{-1} for the amide III structure, and protein backbone modes are observed between 900 and 1100 cm^{-1}, although the signals are of low intensity. Similar results are observed on binding of other ligands to HSA [35,36].

3.2.2. Amide I band of HSA–TiO_2

The fitted band of amide I using Gaussian models (Fig. 10) shows that the adsorbed protein on titanium oxide surface contains 48% α-helix (1652 cm^{-1}), 30% of β-sheet (1671 cm^{-1}) and ~13% of random coil (1635 cm^{-1}) (Table 1). In comparison, the amide I band of free HSA (Fig. 8A), is deconvoluted into an α-helix band at ~1654 cm^{-1} (55%) of with the remaining being mostly β-sheet (22%) and ~(11%)

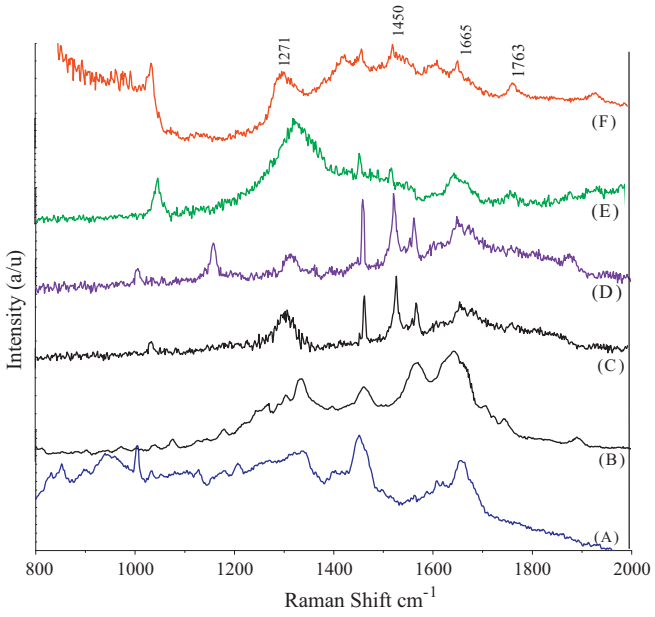

Fig. 8. Raman spectra of HSA powder (A), and HSA adsorbed on TiO_2 (B) [dark control], HSA adsorbed on stainless steel after 30 min UV-B (C) [light control], HSA adsorbed on TiO_2 surfaces after 30 min UV-A (D) and HSA adsorbed on TiO_2 after 30 min UV-B (E).

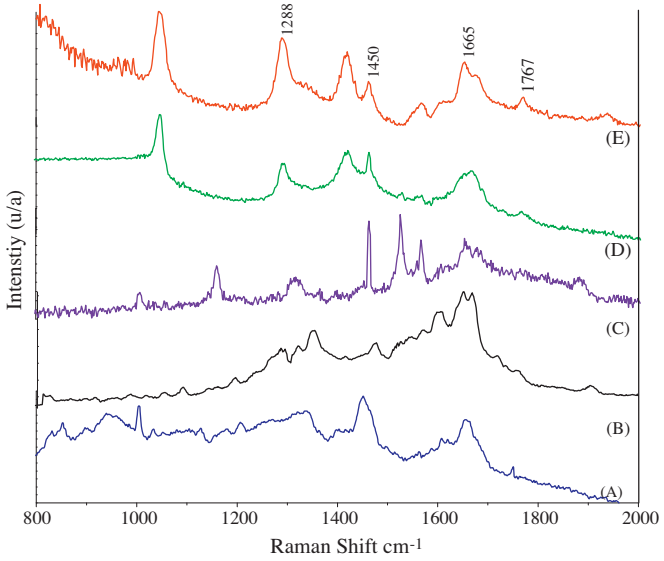

Fig. 9. Raman spectra of HSA powder (A), and HSA adsorbed on $AgTiO_2$ (B) [dark control], HSA on stainless steel after 30 min UV-B (C) [light control], HSA on 4.7 at.% $AgTiO_2$ after 30 min UV-A (D) and HSA on 4.7 at.% $AgTiO_2$ after 30 min UV-B (E).

for random coil (Table 1). By comparing these results with native protein [37,38] (Table 1), it can be inferred that the secondary structure of HSA has been partially disordered due to the binding of HSA to TiO_2.

3.2.3. Raman of HSA–Ag–TiO_2

Following adsorption of the HSA onto the Ag–TiO_2, there is a marked enhancement of the Raman signal and the band intensity increased by up to a factor of 15 in comparison to HSA adsorbed on a TiO_2 surface. The amide I is partially obscured by enhancement of aromatic modes. Surface enhanced Raman (SERS) is observed and is probably due to selective adsorption of the HSA on the silver [39,40].

Fig. 9B shows the Raman shift of HSA adsorbed onto 4.7% (at.) Ag–TiO_2. A band is observed with a maximum near ~1284 cm^{-1} which is attributed to β-sheet and random conformations of amide III mode, whereas a strong band at 1308 cm^{-1} is observed which can be assigned to β-turn and a weak band at ~1340 cm^{-1} which corresponds to the symmetric vibrations of C–H and tryptophan vibrational modes [41]. The observed peak at 1450 cm^{-1} corresponds to the asymmetric bending of CH_3 and CH_2 groups and the peak at 1418 cm^{-1} can be attributed to the C=O stretch of ionized carboxyl groups (COO^-) of aspartic and glutamic acid and side chain vibrations of the imidazole ring of histidine [42].

The backbone skeletal stretch region is found between ~870 and 1150 cm^{-1}, originating mostly in the C_α–C, C_α–C_β, and C_α–N stretches. Also, a weak broad band was observed at ~512 cm^{-1} which may be assigned to the disulphide bridges between cysteine residues (not shown).

3.2.4. Amide I band of HSA–Ag–TiO_2

The various conformational contributions to the amide I bands between 1600 and 1700 cm^{-1} can be de-convoluted by fitting the envelope to Gaussian Lorentzian models. The random coil, α-helix and β-sheet components can be identified on the basis of the amide I Raman components at around 1634, 1654 and 1669 cm^{-1}, respectively, while the bands in the 1680–1690 cm^{-1} region reflect the contribution of β-turn [43–46].

For HSA adsorption on Ag–TiO_2, the de-convoluted band at ~1634 cm^{-1}, which can be assigned to the random conformation, increases relative to the band at ~1654 cm^{-1} (α-helix region) with

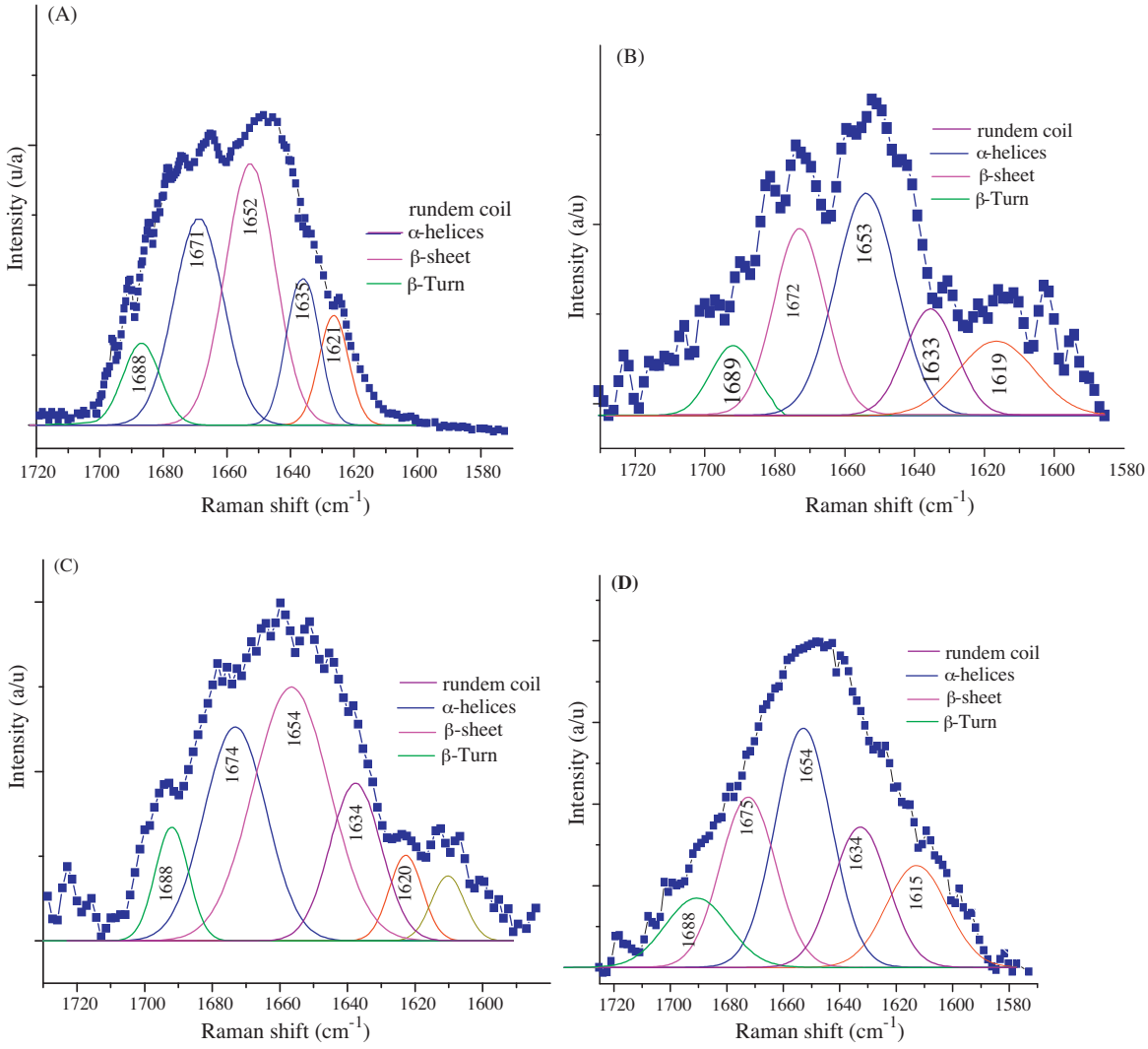

Fig. 10. Raman shift analysis of amide I of HSA adsorbed on: TiO_2 (A) [dark control], stainless steel [light control] (B) and TiO_2 (C) and 4.7 at.% $AgTiO_2$ (D), followed by irradiation with UVB for 30 min.

increasing Ag loading on the TiO_2 (Table 1 and Fig. 10). This indicates that adsorption onto the Ag–TiO_2 results in a change in the protein conformation from α-helix toward β-sheet, (Table 1).

Following the adsorption of HSA, the surface of the TiO_2 and Ag–TiO_2 samples were analysed by XPS. The N 1s signal indicates the presence of the protein [44,47] and the C 1s band intensity was markedly increased, along with a reduction in the Ti 2p and Ag 3d intensities, as compared to clean TiO_2 and Ag–TiO_2 films (Fig. 3). This is further evidence for HSA adsorption [9]. A weak band was observed at 164.1 eV in the high-resolution analysis of the S 2p which can be attributed to sulphur atoms in cysteine) [22].

High resolution analysis of the C 1s peak after adsorption of protein was quite different from the samples prior to protein adsorption. The deconvolution of the C 1s peak gave four different bands at ~285.1, 286.7, 288.4 and 289.5 eV, which correspond to carbon atoms in various environments i.e. (C–C) saturated hydrocarbon groups, (C–NH) amine groups, the peptide bond (C=O–NH) and acidic groups (C–COO–), respectively (Fig. 10A). The amount of HSA bound to the surfaces can be related to the C 1s peak intensity. Following adsorption of HSA, the N 1s spectra were found to have a three different Gaussian bands corresponding to ionic amino group $–NH_3^+$, peptide bond (OC–NH) and the NH_2 groups with binding energies of 401.8 eV, 400.5 eV, and 399.3 eV (Fig. 10). The neutral peptide nitrogen peak and NH_2 peaks dominate the N 1s spectrum, contributing more than 90% of signal [5]. The O 1s band after protein adsorption is similar to that without protein, suggesting that the most of the signal is attributable to metal oxides and surface OH groups (Fig. 10).

In order to determine the change of surface topography upon adsorption of HSA, onto TiO_2 and Ag–TiO_2 films, AFM was performed. The uncoated TiO_2 thin film showed a homogeneous distribution of small clusters or grains of TiO_2 Fig. 6(A*). In case of the TiO_2 film the R_q value changed to (29.1 ± 2.4) nm from (23 ± 2.7), This value of rms is similar to results quoted by Stranak et al. [48]. AFM showed that R_q values increased following protein adsorption, specifically for 4.7% (at.) Ag–TiO_2 the R_q changed to (32.0 ± 2.3) nm from 21.2 ± 1.6 nm, Fig. 6(B*). Consider giving the errors and mentioning the significance of the increase.

3.2.5. UV-photocatalytic degradation of HSA

To assess the ability of TiO_2 and TiO_2–Ag to photocatalytically degrade the adsorbed protein, the films were irradiated with UV-A [365 nm] or UV-B [320 nm]. Fig. 8 shows the Raman shift of HSA in various situations without the presence of Ag, before and after irradiation with UV light. The strong protein bands, amide I and amide III, are centred in the control spectrum at 1660 cm^{-1} and 1281 cm^{-1}, respectively. The essential spectral components of the amide I band are the random-coil structure

between (1634 and 1638) cm^{-1}, the α-helix (1650 and 1655) cm^{-1}, the β-sheet between (1665 and 1678) cm^{-1}, and the β-turn 1685 and 1696 cm^{-1} [45,46]. The deconvoluted analysis of amide I show a series of overlapping bands assigned to a mixture of β-turns, α-helix, β-sheets and random coil structures. The behavior of the β-sheet and α-helix components (respectively at 1673 cm^{-1} and 1653 cm^{-1} in the light control sample) is particularly significant because some interesting shifts after UV-B irradiation are revealed. The band at 1652 cm^{-1} which return to α-helix well shifted to 1654 cm^{-1}, and as same mode the β-sheets pick was shifted from 1672 to 1674 cm^{-1}. As well following UV-B exposure, new features at 1763 cm^{-1} and 1767 cm^{-1} appeared in the Raman spectra for HSA on TiO_2 and 4.7% Ag–TiO_2 surfaces, respectively (Figs. 8 and 9).

According to the literature, HSA contains more than 10% at. of aspartic and glutamic amino acids [49], and there should be a band detected around ~1765 cm^{-1}, but there was no significant peak present following adsorption of HSA on the surfaces. Following UVB irradiation, there was an increase in the intensity of the ~1765 cm^{-1} and this assigned to a C=O bond, as compared with the same protein without irradiation of UVB (Fig. 9b).

Colthup et al., investigated the Raman signal of a γ-carboxylic acid monomer and assigned a band located between (1800 and 1740) cm^{-1} [50]. In addition, Strehle et al. reported on a similar band for fibrinogen adsorbed on TiO_2 which they interpreted as C=O stretch mode of anionic carboxylate bonded to TiO_2. The ability of the protein to bind via its side chains to the TiO_2 varies with conformation [51]. In α-helix conformation, because of the relative orientation of the side chains, binding is expected to be weak to TiO_2. However for random coil and β-sheet conformation the binding strength is expected to be increased. Therefore the relative intensity of 1765 cm^{-1} mode is a useful measure of protein structural change and surface binding.

UVB-photocatalysis causes peptide hydrolysis, releasing α-carboxyl groups which appear at ~1740 cm^{-1}. This indicates that the new peak at ~1765 cm^{-1} might be selected as a marker band for protein degradation in which the intensity changes are due to binding of free carboxyl either following peptide cleavage or gross conformation change in the protein [52].

De-convolution of the XPS C 1s band following UVA irradiation of the HSA on the Ag–TiO_2 (4.7 at.%) sample is shown in (Fig. 12). One can see that the both FWHM and intensity changed compared with the C 1s band before irradiation (Fig. 11). The band area at ~289.3 eV was increased with a decrease of peptide bond peak (288.2 eV), as compared with the C 1s of HSA on Ag–TiO_2 without UV irradiation. This may indicate that peptide cleavage is occurring to form a free carboxylic acid [50].

The surface morphology was investigated by AFM to understand the influence of protein adsorption and UV treatment on the surface topology. The surface roughness for samples decreased following UV-B irradiation as compared with same samples before irradiation (Table 2). The R_q value was reduced to (13.6 ± 2.2) nm and (15.2 ± 2.4) nm for HSA onto TiO_2 and 4.7% Ag–TiO_2, respectively Fig. 6 (A″ and B″). This data may indicate that the protein confor-

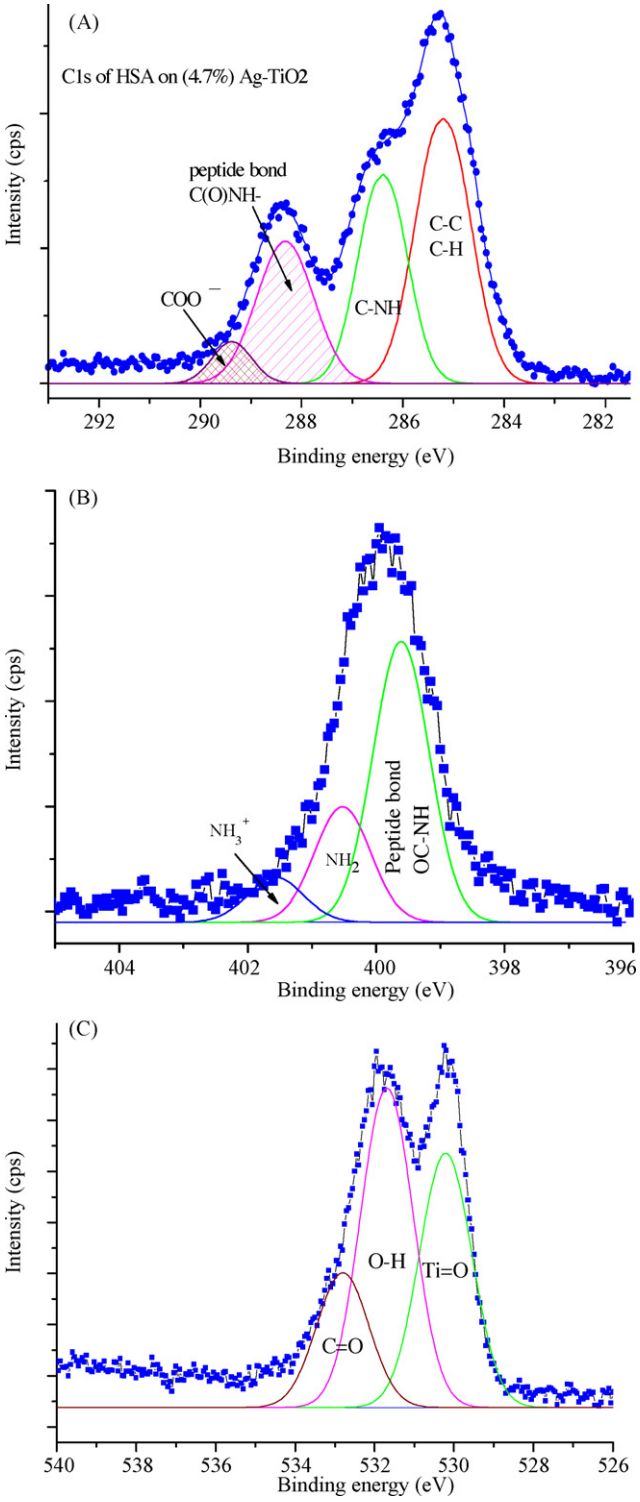

Fig. 11. XPS spectra of C 1s (A), N 1s (B), O 1s (C) of HSA adsorbed on 4.7 at.% Ag–TiO_2.

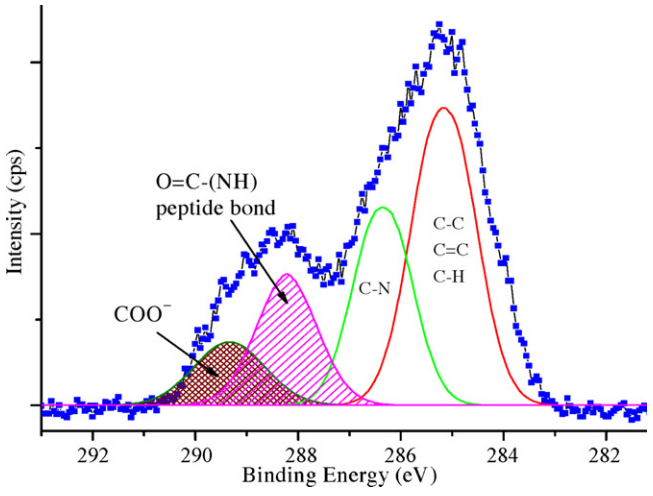

Fig. 12. deconvolution of C 1s band of HSA adsorbed on 4.7 at.% Ag–TiO_2 following UVB irradiation.

Table 2
Roughness values (rms (R_q)) for surface of samples before and after attachment of HSA and after treatment use UV-B.

Sample	Root mean square [rms] (R_q) (nm)		
	Before attachment of HSA	After attachment of HSA	Exposure of UV-B on attached HSA
TiO_2	23.2 ± 2.7	29.1 ± 2.4	13.6 ± 2.2
4.7 at.% Ag–TiO_2	21.2 ± 1.6	32.0 ± 2.3	15.2 ± 2.4

(±): Represent the values calculated standard deviation.

mation became increasingly flat due to increased surface binding of side chain residues as the protein undergoes α-helix to random coil and β-sheet conformation due to cleavage of protein bonds or removal of protein from surface [53].

4. Conclusion

TiO_2 thin films were prepared using magnetron sputtering and Ag–TiO_2 films were prepared by the photocatalytic reduction of Ag metal onto the surface of the TiO_2. After annealing of TiO_2 films at 430 °C for 3 h, the films exhibited the characteristic diffraction peaks due to the anatase phase with no rutile. Examination of Ag–TiO_2 films showed that atomic percentage of Ag increased with increasing photocatalytic treatment time. XPS showed the majority of deposited silver was in Ag^0 form with small amount of Ag^+ ions. The adsorption of HSA onto surfaces of TiO_2 and Ag–TiO_2 and the atomic ratio of silver tended to change the protein conformation by shifting of amide III toward higher wavelength, and reduce of α-helices mode in amide I band indicative of enhanced of β-sheet and random coil formation (as compares with native protein). A new band at ∼1765 cm^{-1} was observed following UV irradiation of the films and can be attributed to C=O str. mode of carboxylate which may arise from photocatalyic peptide bond cleavage and increased binding of these groups to the surface leading to the conformational change of the protein.

Acknowledgments

This work was supported by SFI under the investigator programme, Award No. 05/IN.1/B30/NS. The authors would like to acknowledge, all staff in the Nanotechnology Integrated Bio-Engineering Centre (NIBEC), University of Ulster, and National Centre for Sensor Research (NCSR), Dublin City University, for assistance with the analysis. CB and TEK gratefully acknowledge the Higher Education Authority for Funding under the Programme for Research at Third Level Institutions.

References

[1] B.B. Zhang, Y.F. Zheng, Y. Liu, Dental Materials 25 (2009) 672–677.
[2] M. Niinomi, Metallurgical and Materials Transactions A 32A (2001) 477–486.
[3] P. Cacciafesta, K.R. Hallam, A.C. Watkinson, G.C. Allen, M.J. Miles, K.D. Jandt, Surface Science 491 (2001) 405–420.
[4] U. Mudali, T.M. Sridhar, B. Raj, Sadhana 28 (3 & 4) (2003) 601–637.
[5] S.R. Sousa, P.M. Ferreira, B. Saramago, L.V. Melo, M.A. Barbosa, Langmuir 20 (2004) 9745–9754.
[6] M. Niinomi, Journal of the Mechanical Behaviour of Biomedical Materials 1 (2008) 30–42.
[7] Y.X. Leng, J.Y. Chen, J. Wang, G.J. Wan, H. Sun, P. Yang, N. Huang, Surface & Coatings Technology 201 (2006) 157–163.
[8] M.B. Casu, W. Braun, K.R. Bauchspie, S. Ker, B. Megner, C. Heske, R. Thull, E. Umbach, Surface Science 602 (2008) 1599–1606.
[9] B. Fenga, J. Wenga, B.C. Yanga, J.Y. Chena, J.Z. Zhaob, L. Heb, S.K. Qib, X.D. Zhanga, Materials Characterization 49 (2003) 129–137.
[10] E.D. Belay, L.B. Schonberger, Annual Reviews Public Health 26 (2005) 191–212.
[11] J.A. Byrne, B.R. Eggins, Journal of Electroanalytical Chemistry 457 (1–2) (1998) 61–72.
[12] D.M. Blake, P.-C. Maness, Z. Huang, E.J. Wolfrum, J. Huang, Separation and Purification Methods 28 (1) (1999) 1–50.
[13] A. Mills, S. Le Hunte, Journal of Photochemistry and Photobiology A: Chemistry 108 (1997) 1–35.
[14] P.S.M. Dunlop, T.A. McMurray, J.W.J. Hamilton, J. Anthony Byrne, Journal of Photochemistry and Photobiology A: Chemistry 196 (2008) 113–119.
[15] A. Makakowski, W. Wardas, Current Topic in Biophysics 25 (1) (2001) 19–25.
[16] H. Szymanowski, A. Sobczyk, M.G. Lipman, W. Jakubowski, L. Klimek, Surface & Coatings Technology 200 (2005) 1036–1040.
[17] H. Yun, J. Li, H.B. Chen, C.J. Lin, Electrochimica Acta 52 (2007) 6679.
[18] J.W.J. Hamilton, J.A. Byrne, C. McCullagh, P.S.M. Dunlop, International Journal of Photoenergy (2008), doi:10.1155/2008/631597.
[19] A. Mills, G. Hill, M. Stewart, D. Graham, W.E. Smith, S. Hodgen, P.J. Halfpenny, K. Faulds, P. Robertson, Applied Spectroscopy 58 (8) (2004) 922–928.
[20] M. Es-Souni, M. Es-Souni, S. Habouti, N. Pfeiffer, A. Lahmar, M. Dietze, C.H. Solterbeck, Advanced Functional Materials 20 (2010) 377–385.
[21] O. Akhavan, Journal of Colloid and Interface Science 336 (2009) 117–124.
[22] H. Yoneyama, T. Torimoto, Catalysis Today 58 (2–3) (2000) 133–140.
[23] X. Wang, F. Prokert, H. Reuther, M.F. Maitz, F. Zhang, Surface & Coatings Technology 185 (2004) 12–17.
[24] W.R. Li, X.B. Xie, Q.S. Shi, H.Y. Zeng, Y.S.O. Yang, Y.B. Chen, Applied Microbiology and Biotechnology (2009), doi:10.1007/s00253-009-2159-5.
[25] O. Akhavan, E. Ghaderi, Surface & Coatings Technology 204 (2010) 3676–3683.
[26] Y. Liu, X. Wang, F. Yang, X. Yang, Microporous and Mesoporous Materials 114 (2008) 431–439.
[27] R. Kumar, S. Howdle, H. Munstedt, Journal of Biomedical Materials Research Part B: Applied Biomaterials 75B (2) (2005) 311–319.
[28] Y. Cao, H. Tan, T. Shi, T. Tang, J. Li, Journal of Chemical Technology and Biotechnology 83 (2008) 546–552.
[29] R. Vinu, G. Madras, Applied Catalysis A: General 366 (2009) 130–140.
[30] A. Roguska, A. Kudelski, M. Pisarek, M. Lewandowska, M. Dolata, M. Janik-Czachor, Journal of Raman Spectroscopy 40 (11) (2009) 1652–1656.
[31] H.W. Wong, S.M. Choi, D.L. Phillips, C.Y. Ma, Food Chemistry 113 (2009) 363–370.
[32] O. Akhavan, E. Ghaderi, Surface & Coatings Technology 203 (2009) 3123–3128.
[33] A.R. Malagutti, H.L. Moura, J.R. Garbin, C. Ribeiro, Applied Catalysis B: Environmental 90 (2009) 205–212.
[34] X. Wu, J. Li, L. Wang, D. Huang, Y. Zuo, Y. Li, Biomedical Materials 5 (2010) 044105, 7pp.
[35] S. Ngarize, A. Adamsb, N.K. Howell, Food Hydrocolloids 18 (2004) 49–59.
[36] L.B. Avalle, O.R. Camara, F.Y. Oliva, Journal of Electroanalytical Chemistry 585 (2005) 281–289.
[37] Z. Jurasekova, A. Tinti, A. Torreggiani, Analytical and Bioanalytical Chemistry 400 (9) (2011) 2921–2931.
[38] H.A. Tajmir-Riahi, Scientia Iranica 14 (2) (2007) 87–95.
[39] O. Inya-Agha, D. Lucey, R.J. Forster, T.E. Keyes, Plasmonics in biology and medicine IV, in: T. Vo-Dinh, J.R. Lakowicz (Eds.), Proceedings of SPIE, vol. 6450, 2007.
[40] A. Kaminska, O. Inya-Agha, R.J. Forster, T.E. Keyes, Physical Chemistry Chemical Physics 10 (2008) 4172–4180.
[41] E.C.Y. Li-Chan, Trends in Food Science & Technology 7 (11) (1996) 361–370.
[42] C.C. Orfanidou, S.J. Hamudrakas, G.D.E. Chryssikos, I. Kamitsos, S.E. Wellman, S.T. Case, International Journal of Biological Macromolecules 17 (2) (1995) 93–98.
[43] H. Torii, M. Tasumi, J. Chem. Phys 96 (5) (1992) 3379–3387, theoretical, IR, http://jcp.aip.org/resource/1/jcpsa6/v96/i5/p3379_s1.
[44] D.M. Brunette, Titanium in medicine: material science, Surface Science (e-Book) (2001).
[45] A. Synytsya, P. Alexa, J. de Boer, M. Loewe, M. Moosburger, M. Wurkner, K. Volka, Journal of Raman Spectroscopy 38 (2007) 1646–1655.
[46] C. David, S. Foley, C. Mavon, M. Enescu, Biopolymers 89 (7) (2008) 623–634.
[47] T. Kesvatera, B. Jonsson, A. Telling, V. Tougu, H.V.E. Thulin, S. Linse, Biochemistry 40 (2001) 15334–15340.
[48] V. Stranak, M. Cada, M. Quaas, S. Block, R. Bogdanowicz, S. Kment, H. Wulff, Z. Hubicka, C.A. Helm, M. Tichy, R. Hippler, Journal of Physics D: Applied Physics 42 (2009) 105204–105215.
[49] D. Shemin, D. Rittenberg, Journal of Biological Chemistry 159 (1945) 439–443.
[50] N.B. Colthup, L.H. Daly, S.E. Wiberley, Introduction to Infrared and Raman Spectroscopy, Academic Press, San Diego, CA, 1990.
[51] M.A. Strehle, P. Rosch, R. Petry, A. Hauck, R. Thull, W. Kiefer, J. Popp, Physical Chemistry Chemical Physics 6 (2004) 5232–5236.
[52] F. Zhang, G.K. Wolf, X. Wang, X. Liu, Surface & Coatings Technology 148 (1) (2001) 65–70.
[53] J. Kuwahara, H. Akisada, T. Kato, N. Nishino, Colloid and Polymer Science 283 (2005) 747–752.